Advances in Environmental Technology 3 (2016) 153-168

Advances in Environmental Technology

journal homepage: http://aet.irost.ir

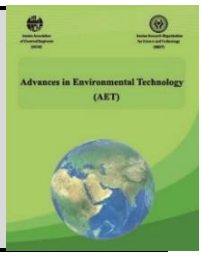

Photocatalytic treatment of spent caustic wastewater in petrochemical industries

Amin Ahmadpour[1], Ali Haghighi Asl[1*], Narges Fallah[2]

[1]*Faculty of Chemical, Gas and Petroleum Engineering, Semnan University, Semnan, Iran*

[2]*Chemical Engineering Department, Amirkabir University of Technology, Tehran, Iran*

ARTICLE INFO

Article history:
Received 13 June 2015
Received in revised form
19 November 2016
Accepted 22 January 2017

Keywords:
Artificial neural networks (ANN)
Design of experiment (DOE)
Photocatalytic wastewater treatment
Spent caustic wastewater
Titanium dioxide

ABSTRACT

In this study, the photocatalytic method was used for treating the spent caustic in the wastewater of Olefin units used in petrochemical industries which contain large amounts of total dissolved solids (TDS). By using the synthetic photocatalyst of suspended titanium dioxide and measuring the chemical oxygen demand (COD) which was reduced in the photocatalyst (lbc) process, the values of COD were modeled and evaluated by means of the Box-Behnken (BBD) and the artificial neural network (ANN) using experimental tests in a double-cylindrical-shell photo reactor. According to the applied calculations, it was found that the artificial neural network was a more suitable method than the experimental design in modeling and forecasting the amount of COD removal. The modeling employed in this research showed that increasing the concentration of the photocatalyst in a state of neutral pH enhanced the COD removal up to the optimal amount of 1.31 g/L without restrictions and 2 g/L with restrictions at the rate of 81% and 79%, respectively. In addition, the study of the parameter effects including oxidizer amount, aeration rate, pH, and the amount of loaded catalyst indicated that all factors except pH had a positive effect on the model; furthermore, if the interactions were neglected, the COD removal efficiency would increase by increasing each of these factors (except pH). In addition, there was no interaction between the aeration and the concentration of the photocatalyst, and the acidic pH was more suitable at low concentrations of the photocatalyst. Besides that, by increasing the pH, the efficiency of removal was reduced when the oxidant was at its low level. The results showed that photolysis and adsorption adoptions had a very small effect on the efficiency of the removal of COD compared to the photocatalyst adoptions, and it was insignificant. In addition, the photocatalytic method had an acceptable capacity for removing the phenol in the wastewater sample, whereas it was inefficient in reducing the sulfide solution in the wastewater.

1. Introduction

The exhaust gases generated in the furnaces of Olefin units in the petrochemical industry contain sulfur compounds which are separated in a flash drum (distillation column**)** by using caustic soda, thus the spent caustic in the wastewater contains sulfur materials which must be disposed of by a suitable treatment. In the process, following the removal of hydrogen sulfide, the toxic and harmful composition of sodium sulfide is observed in the wastewater. This caustic hazardous waste has a high acidity and contains sodium-free and inorganic salt compounds, sulfide, and hydrocarbons. The caustic sodium should be filtered because their high concentrations poison the microorganisms used in biological wastewater treatment [1]. Given that the spent caustic found in the wastewater

*Corresponding author. Tel: +98-2333654138
E-mail address: ahaghighi@semnan.ac.ir

contains a wide range of hydrocarbons, the photocatalytic oxidation method can be a rational and effective option for the primary degradation of pollutants before biological treatment and after physical pre-treatment. The pollution from sulfide is toxic, highly corrosive, and damaging to equipment. The presence of sulfide pollution in the wastewater results in generations of insoluble metal deposits. By using the photocatalytic oxidation method with oxidizing materials such as oxygen or hydrogen peroxide, the sulfide, sulfide compounds and hydrocarbon compounds can be reduced and brought down to specified standards. The photocatalytic degradation of these compounds depends on the type and composition of the catalyst, light intensity, concentration of the raw material, amount of catalyst, pH of reaction solution, utilizing the method of catalyst, and calcination temperature. Determining the effect of the various factors on the photocatalytic efficiency is very important for designing an industrial scale treatment process [2]. So far, numerous studies have been conducted on the treatment of wastewater containing spent caustic. Mara et al. (2000) studied the treatment of caustic wastewater by using the wet air oxidation method. They decreased the amount of COD from 72,000 to 15,000 mg/L by using 0.2m^3 of caustic wastewater and diluting it with 0.4m^3 of water at 260ºC at a pressure of 90 bar [3]. H. Sheu et al. (2001) successfully removed more than 94% of the COD from the wastewater by using the combination of neutralization and the Fenton's reagent process. Their study showed that this process has the ability to reduce the COD from 40,000 mg/L to 1400 mg/L as well as reducing the sulfides from 19000 to 1400 mg/L. In addition, adding the Fenton process to the above sequence further reduced the COD, up to 150 mg/L [4]. Rodriguez et al. (2008) employed the electro-generated Fenton's reagent in their research. They reported a COD removal of 95% at a pH of 4 and a temperature of 40ºC by using 100 mg/L of iron [5]. Nunez et al. (2009) treated the spent caustic wastewater by using the electrochemical oxidation process and successfully removed 93% of the COD [6]. Yus et al. (2004) reported 68% of COD removal by using a combination process of UV/H_2O_2 beside $UV/H_2O_2/O_3$. In the same study, the process of UV/H_2O_2 had an efficiency of 44% in COD removal [7]. Hawari et al. (2015) likewise studied the treatment of caustic wastewater in various processes. They reported 99% of sulfide removal at a pH of 5.1; 98% of COD removal was also observed in this study. It was also reported that oxidation through H_2O_2 was able to remove 89% of the COD at a pH of 2.5 as well as the consumption of 19 Mol/L of the hydrogen peroxide [8]. Abdullah et al. (2011) used the photo-Fenton oxidation process to investigate the treatment of synthetic spent caustic wastewater. They reported 92% of COD removal and a 98% decrease in the sulfide under optimal conditions [9]. C. Chen et al. (2012) examined the treatment of wastewater with genuine spent caustic with COD equal to 25,000 by the conventional wet air oxidation method and catalytic wet air oxidation. They reported a reduction of 75% and 95% for the conventional and catalytic method, respectively [10]. M. Alaiezadeh (2012) studied the COD reduction of the spent caustic wastewater treatment of the South Pars gas refinery by using the electrical coagulation method. The greatest efficiency of the process (91%) was carried out at an effective time of 105 minutes by diluting the wastewater to a water volume ratio of 2, a pH of 9, a current density of 62.8 milliamps per square centimeter (mA/cm^2), and 1.32 g/L of $FeSO_4$ material [11].

In photocatalytic systems, various parameters such as temperature, pH, amount of catalyst, etc., impact the efficiency of the photocatalytic degradation process. The existence of different factors that examine the photocatalytic reactions usually leads to an increase in the number of tests, which results in high costs and is also time consuming. For this purpose, the use of experimental design can be an appropriate option. Response surface methodology (RSM) is among the most common designs that can be employed for performing the experimental design of each project. Two renowned designs that are useful in RSM are central composite design (CCD) and Box Behnken [12]. To our knowledge, there are no studies that have used artificial neural network modeling for the removal or reduction of COD in wastewater containing spent caustic. The artificial neural network is a model for data processing that is made like the human brain by imitation of the biological neural networks. The key element of this model is the new structure of the data processing system that has been formed by a large number of elements (neurons) with internal and strong communications that work harmoniously together to solve specific problems. In general, the learning ability is the most important feature of an intelligent system, making it more flexible and easier to program; therefore, such a system can better respond to new issues and equations. Algorithmic methods are not suitable for implementing these features in computers; as a result, the methods should be based on the same biological models. The data structure called a node is designed and can act as neurons in these networks by helping the programming knowledge. Then, the network is trained by generating a network between these nodes and applying a learning algorithm [13]. The synthesis of nanoparticles from the liquid phase has been repeated frequently because it is easy, manageable and efficient, especially in controlling the size, composition and sometimes the shape of the particles. In general, chemical synthesis contains methods that include the liquid phase deposition. These methods differ from the mechanical methods (top-down approach) and the physical methods (methods of gas-phase synthesis). In some texts, these methods are named the Wet Synthesis Methods or the Solution Phase Synthesis. It can be said that in this status, the solution species are converted to an insoluble chemical form. The chemical synthesis of the

nanoparticles provides the nanostructure engineering techniques as well as the surface modification. Furthermore, the synthesis methods in the liquid phase can manufacture the thin-film with nanotechnology like the physical methods and unlike many mechanical methods. The following are various methods of producing the nanoparticles in the liquid phase: Sol-Gel, microemulsion, hydrothermal, thermal decomposition, deposition synthesis by using microwave, deposition synthesis by using sonication, chemical precipitation, and solvothermal [14]. In this paper, the photocatalytic degradation of spent caustic has been studied. Based on our knowledge, it is an interesting and new method for this type of waste. Titania was synthesized with high purity and applied for the degradation of spent caustic waste in an effective way to reach a high level of process efficiency. Also, this research attempted to apply an innovative statistical method for achieving the best and most reliable results.

2. Materials and methods

2.1. Characterization of raw wastewater

The output of the neutralization segment of the spent caustic in the wastewater produced in the Olefin unit of petrochemical industries was selected as the input wastewater sample in the photo reactor. The characteristics of the wastewater are shown in Table 1.

Table 1. Major characteristics of the actual and used wastewater as the raw material for photocatalytic reactor

Characteristic	Measurement	Amount
COD	mg/L	1280
BOD	mg/L	615
pH	-	7.3
Phenol	mg/L	4.7
TDS	mg/L	89000
Na_2S	mg/L	7.8

2.2. Required chemical materials

The chemical materials used in this study included the following: the prepared auxiliary oxidant of hydrogen peroxide acquired from the Merck company with a concentration of 35% (volume); the prepared sulfuric acid of 98% (weight) and caustic soda of 35% (weight) from the Merck company (to adjust pH); the required chemical materials (dichromate potassium, sulfate of mercury, silver sulfate and potassium hydrogen phthalate) to measure the COD parameter; the Phenols Test Kit; the required chemical materials (hydrochloric acid, copper sulfate, sodium sulfide) to measure the parameters of sulfide solution; and the required material (isopropanol, ethylene glycol, titanium tetra isopropoxide) for the synthesis of the titanium dioxide photocatalyst.

2.3. Synthesis of the titanium dioxide photocatalyst

The solvothermal method was used in this study for the synthesis of titanium dioxide. First, 5 ml of titanium tetra isopropoxide (TTIP) was dissolved in 11.5 ml of isopropanol and this solution was stirred. Then this solution was added to ethylene glycol and transferred into the autoclave for 12 hours in a furnace at a temperature of 240ºC. Subsequently, the furnace was turned off and the content of the autoclave reached ambient temperature. Then, this material was centrifuged, washed several times with distilled water, and dried at a temperature of 50℃ for 24 hours.

2.3.1. XRD analysis

The structure of synthesized TiO_2 nanoparticles via XRD analysis is shown in Figure 1. It can be seen that the XRD reflections of the photocatalyst synthesis of this research overlap well with commercial pattern reflections of the titanium dioxide p-25 from the Degussa Company and also with reference pattern reflections of its Anatase phase (JCPDS Cards 33-0664) (major reflections: 25.3º, 37.8º, 48.2 º, 54.0º and 62.7º) [14]; an impurity peak is not observed at all. Notably, the synthesized peak pattern is sharp and it is similar to commercial patterns of titanium dioxide which indicates the high crystallinity of the catalyst. The Scherrer equation was used to calculate the crystal size and was found to be 21.4 nanometers.

$$d_C = \frac{B\lambda}{\beta \cos\theta} \quad (1)$$

where B is the constant number between 0.9 to 1.00, λ is the wavelength of the device source (by Angstrom unit) equal to (1.5406), β is the width of the half maximum of peak or FWHM (in Radian), and Cosθ is the cosine of an angle that the desired peak is located in. The obtained d_c from the Scherrer equation is the size of the crystal in terms of Angstrom.

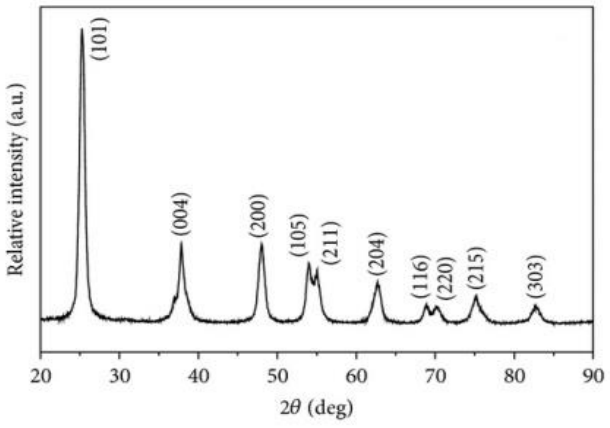

Fig. 1: Plot of XRD for synthetic TiO2 photocatalyst

2.3.2. SEM analysis

The SEM test was done via an electron microscope to examine the surface morphology and nanoparticle size. The image of the synthesized titanium dioxide nanoparticles is shown in Figure 2 in the scale of one micrometer. The comparison of this image with the sample image of the commercial titanium dioxide p-25 of the Degussa Company represents the similarity of the two structures. This image confirmed the spherical and nearly identical structure of the nanoparticles. In this test, the average particle size in the synthetic photocatalyst was 22 nm and was calculated by Microstructure Measurement software. The obtained particle size from SEM was not the same as the calculated size of the crystal in XRD, and it indicated that a particle was formed by gathering the number of crystals together.

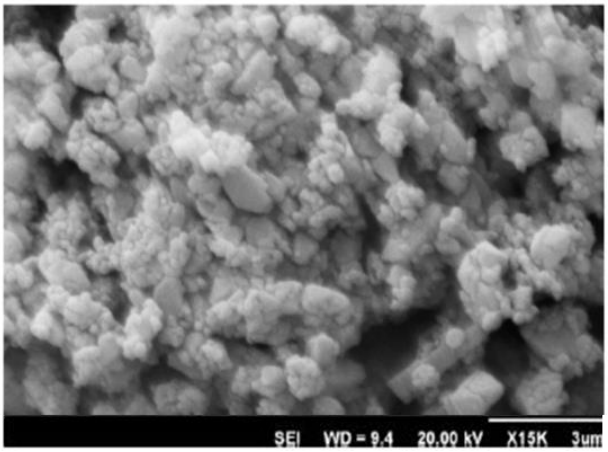

Fig. 2. SEM Image of synthetic TiO_2 photocatalyst

2.3.3. Determination of the pH of the point of zero charge (pH_{pzc}) in photocatalyst

At this point, the photocatalyst surface load was neutral through the performance way of a test which is presented by Utrilla et al. [15] and determined the range of adsorption according to the cationic or anionic nature of the wastewater. The value of this parameter was 6.8 for the synthetic titanium dioxide photocatalyst Figure 3.

2.4. Photo reactor specifications

In this study, all the oxidation reactions were carried out discontinuous in atmospheric conditions by a double-cylindrical-shell photo reactor with a stirrer. The related photocatalyst was used in the photocatalytic degradation process in a slurry solution. The slurry reactor had a double-cylindrical-shell that was made of 304-stainless steel. In this reactor, eight 16 watt UV-C bubble lights (made by the Netherlands-Philips Company) were used with an eight quartz glass sheath. In fact, for positioning the lamps inside the photo reactor, some quartz pipes with the size of 45 × 2 cm were vertically used in the intended places. The distance of the lamps from each other should be the same for generating uniform light intensity in the reactor. During the test, aluminum foil was placed on the lid of the reactor to avoid light emission to the surroundings. Viton gaskets were also used to block the surroundings of the quartz glass after reactor installation. A blade stirrer with three rows of paddle shaped blades was used for stirring the reaction solution, and this 200 RPM blade stirrer was equipped with a 12 volt DC Electro-Motor. The required oxygen was provided via aeration by means of a Heila compressor with the capacity of 35 liters per minute; after measuring by a Rotameter, the oxygen was injected through an annular aquarium sparger in order to create smaller bubbles and proper distribution of air into the system. The photo reactor was equipped with a jacket cooling water system to control the temperature. The range of the recorded temperature was between 26 to 27ºC in all stages of the test which showed the isothermal reaction conditions. This photo reactor is schematically shown in Figure 4.

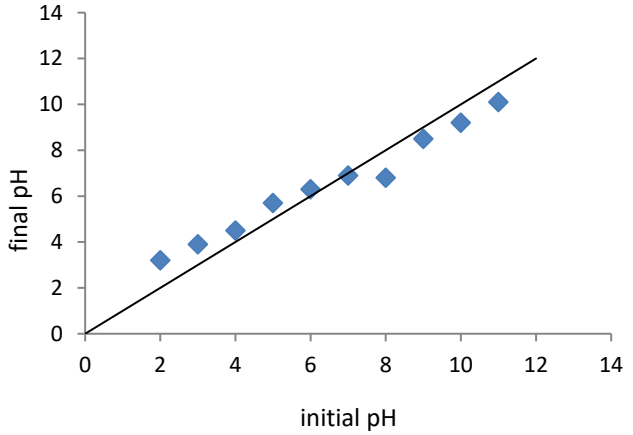

Fig. 3. Determination of pH_{pzc} for synthetic titanium dioxide photocatalyst

2.5. Test method

In this study, a sample was first taken from the reactor before the photocatalytic reaction and its COD value was determined in order to study the effect of the photocatalytic reaction during testing; then, it was compared with the adsorption process (absence of light) and photolysis (presence of light). Then, under the determined DOE conditions of 90 minutes and at intervals of 10 minutes, 2mL of the reactor contents was taken and its COD was determined in the photocatalytic reaction. The lab method Standard No. 5220 APHA was used for this purpose. The 5530-D standard APHA laboratory method was used to measure the amount of phenol in the wastewater sample; the methylene blue method was used to determine the amount of dissolved sulfide in the wastewater [16]. In this study, the efficiency of the photocatalytic removal of COD in the 90th minute was selected as the response (objective function) and it can be calculated by using Equation (2).

$$\%\ \text{removal efficiency} = \frac{C_0 - C}{C_0} \times 100 \quad (2)$$

where C and C_0 are the COD parameters at the beginning of the photocatalytic process (moment of turning on the lamps) and at the sampling time of the 90th minute, respectively [17].

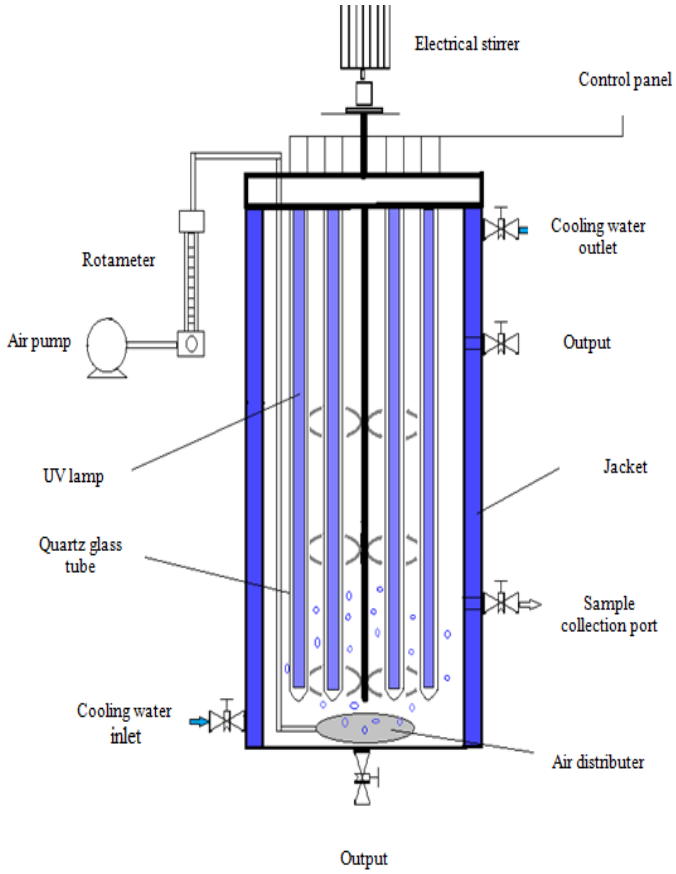

Fig. 4. Schematic diagram of the photoreactor

2.6. Design of experiment (DOE) and Artificial neural network (ANN)

A two-level factorial screening method was used in order to determine the main factors of the photocatalytic process which included using a titanium dioxide photocatalyst synthesis of the research and Design Expert software. Four main factors were determined: (A) photocatalyst concentration, (B) pH, (C) the concentration of auxiliary oxidant (hydrogen peroxide), and (D) the aeration rate. The Response Surface Method (RSM) of the Box-Behnken type was used for modeling (all of the analysis was done at a 95% level of confidence). In this method, a polynomial was used according to Equation (3) for the relationship between the response and independent variables.

$$y = \beta_0 + \sum_{i=1}^{k} \beta_i x_i + \sum_{i=1}^{k} \beta_{ii} x_i^2 + \sum_{1 \le i \le j}^{k} \beta_{ij} x_i x_j + \quad (3)$$

where (y) is the response variable or the percentage of the COD removal, (β_0) is the constant value of the polynomial, (β, β_{ii}, β_{ij}) are the regression coefficients of interaction, (x_j, x_i) are the independent variables, and (ε) is the random error rate. In this design, 30 experimental tests were used. The aim of the DOE in the present study was the optimization of the removal process of COD in the wastewater sample. The range and level of selective factors were collected in Table 2.

Table 2. Range and level of selective factors

Levels code of each variable		Sign	Factor
High (+1)	Low (- 1)		
Photocatalyst concentration (g/L)	A	0.5	2
pH	B	4	10
Oxidizer concentration (ppm)	C	0	300
Aeration intensity (l/ min)	D	0.5	4

This study used the experimental data in the established neural network model, which includes input layer, hidden layer and output layer. According to the selected input variables, the network structure is shown in Figure 5. In the artificial neural network subject, Equations 4 to 7 were used to determine the adjusted correlation coefficient (Adjusted R^2), Mean Absolute Error (MAE), Absolute Average Deviation (AAD) and Root Mean Squared Error (RMSE). In these equations, (K) is the number of input variables, (n) is

the number of data, and (X_{im} and X_{ip}) are the predicted values respectively, and arise from the model for the response variable. MATLAB software was used for modeling in this study [18].

$$R^2_{adj.} = 1 - \left[(1 - \mathrm{R}^2)\frac{\mathrm{n}-1}{\mathrm{n}-\mathrm{K}-1}\right] \quad (4)$$

$$RMSE = \sqrt{\frac{\sum_{i=1}^{n}\left(X_{im} - X_{ip}\right)^2}{n}} \quad (5)$$

$$MAE = \frac{\sum_{i=1}^{n}\left|X_{im} - X_{ip}\right|}{\mathrm{n}} \quad (6)$$

$$AAD = \left\{\frac{\sum_{i=1}^{n}\left(\left|X_{im} - X_{ip}\right|/X_{im}\right)}{\mathrm{n}}\right\} \times 100 \quad (7)$$

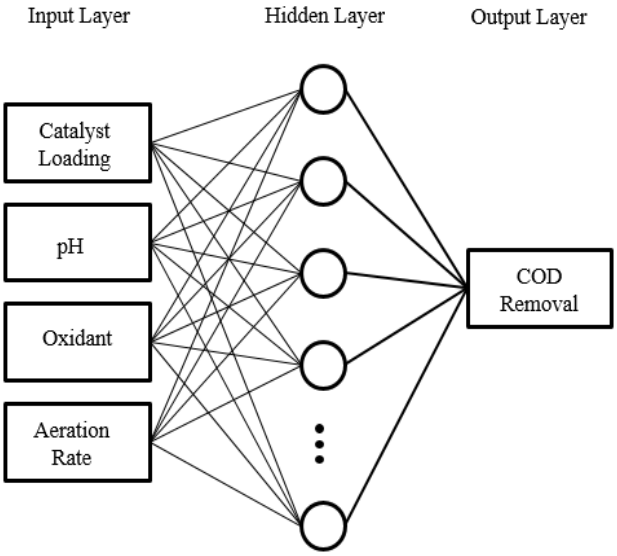

Fig. 5. Structure of the designed neural network

3. Results and Discussion

Both the modeling of the design of experiment and the artificial neural network method showed the validity of the results arising from it; the results are shown in Table 3.

3.1. Modeling of Design of Experiment

The output arising from the modeling was searchable by means of the Design Expert software in the form of variance analysis and diagnostic plots.

3.1.1. Analysis of Variance (ANOVA)

To interpret the relevant model, statistical tests such as ANOVA were used. The obtained model was based on a second-degree polynomial in which unimportant polynomials have been statistically removed by removing the lead method. The second-degree polynomial equation in the form of coding parameters is similar to Equation (8) for this design.

$$R=+74.93+11.75A-8.23B+14.26C+10.76D+8.93AB-13.41AC-7.94AD+14.48BC-6.65CD-3.14A^2-14.35B^2-5.59C^2-9.84D^2 \quad (8)$$

As can be seen from Table 4, the obtained model is statistically valid. This can be well understood of p-values that are less than 0.05. In addition, BD polynomial (interaction of aeration and pH) has been removed because it is meaningless.

3.1.2. Diagnostic Plots

The diagnosis part in the design of experiments software will be examined to ensure the accuracy of the model and to fix its defects. Some of these plots are indicated as follows.

3.1.2.1. The graph of actual and predicted data

Figure 6 shows the actual data plots (experimental) versus the predicted data of the model. As can be seen from the model, the calculated data error from the model and experimental data are acceptable with a good approximation.

3.1.2.2. Cox-Box plot

The Box-Cox plot helped in determining the most appropriate power transformation to apply to the response data. Most data transformations can be described by the power function, σ= fn (μ^{α}), where sigma (σ) is the standard deviation, mu (μ) is the mean, and alpha (α) is the power. Lambda (λ) was 1-α in all cases. If the standard deviation associated with an observation was proportional to the mean raised to the á power, then the transforming of the observation by the 1 - α (or λ) power gave a scale satisfying the equal variance requirement of the statistical model. This plot facilitated the diagnosis of the most appropriate power transfer function in order to apply the response. In fact, this plot was used to determine the appropriate power to transform the model. Here, the proposed transformation will be obtained based on the best lambda variable value that is provided by the software on the minimum point of the produced curve by the logarithm of the sum of the residuals. The lowest point in the plot was the best lambda value in which at least the sum of the left residuals was created in the transformed model. When the ratio of maximum to minimum response value was greater than three, there was more ability to improve the model by using the power function (Figure 7).

Table 3. Design of experiment and Artificial neural network by using synthetic titanium dioxide

Run	A: Catalyst Loading (g/L)	B: pH	C: C_{H2O2} (ppm)	D: Air ($lmin^{-1}$)	Response COD Degradation% Exp.	Response COD Degradation% DOE	Response COD Degradation% ANN
1	1.25	7.00	150.00	2.25	74	74	75
2	1.25	7.00	300.00	0.50	71	69	70
3	2.00	10.00	150.00	2.25	67	69	67
4	1.25	7.00	150.00	2.25	76	74	75
5	2.00	7.00	300.00	2.25	81	78	81
6	0.50	10.00	150.00	2.25	32	29	32
7	1.25	10.00	0.00	2.25	20	18	20
8	0.50	7.00	150.00	0.50	30	32	30
9	1.25	7.00	300.00	4.00	77	78	77
10	0.50	7.00	0.00	2.25	24	27	24
11	1.25	4.00	150.00	0.50	47	48	47
12	2.00	7.00	150.00	0.50	73	70	73
13	1.25	7.00	0.00	0.50	28	27	28
14	1.25	7.00	0.00	4.00	62	62	62
15	1.25	7.00	150.00	2.25	73	74	73
16	1.25	7.00	150.00	2.25	75	75	75
17	2.00	7.00	0.00	2.25	77	77	77
18	0.50	7.00	150.00	4.00	68	68	68
19	1.25	10.00	300.00	2.25	75	76	75
20	1.25	4.00	0.00	2.25	65	63	65
21	0.50	4.00	150.00	2.25	65	65	65
22	1.25	4.00	300.00	2.25	62	63	62
23	1.25	10.00	150.00	0.50	31	32	31
24	0.50	7.00	300.00	2.25	81	82	79
25	1.25	10.00	150.00	4.00	52	53	52
26	1.25	4.00	150.00	4.00	71	70	71
27	2.00	7.00	150.00	4.00	79	76	76
28	1.25	7.00	150.00	2.25	77	75	75
29	2.00	4.00	150.00	2.25	65	69	65
30	1.25	7.00	150.00	2.25	75	75	75

3.1.3. Interaction plot of photocatalyst and pH value parameters

The interaction of the studied parameters on the removal rate was examined with the help of the three-dimensional response surface plots and contour line diagrams. In this study, the interaction between the photocatalyst and the pH values was studied at different levels of the auxiliary oxidant value. Figure 8 and the contour lines of Figure 9 show the interaction between the initial solution pH and the loaded catalyst in the process at three different levels of oxidants (0,150,300 ppm) and mid-level of aeration intensity factor. The higher concentrations of photocatalyst required a higher pH to prevent aggregation. But generating the hydroxyl radicals depended only on the positive whole reaction with the water molecule or hydroxide ions, which the lack of the second resource for generating the hydroxyl radical (hydroperoxyl radical) was compensated by increasing the amount of the photocatalyst. In the alkaline pHs, the pollutant adsorption became less and therefore, the rate of degradation was reduced according to the created negative load on the photocatalyst surfaces. PH was one of the parameters that played a fundamental role in the photocatalytic processes. The existence of high levels of antioxidants led to maintain a great amount of the removal rate. Generally, photocatalytic processes have higher efficiency in low pH. The existence of antioxidants with high levels prevented the emergence of a high pH effect on the process which meant that pH and oxidant had positive

interaction in the process. In addition, as pH increased, the efficiency decreased when the oxidant was at a low level.

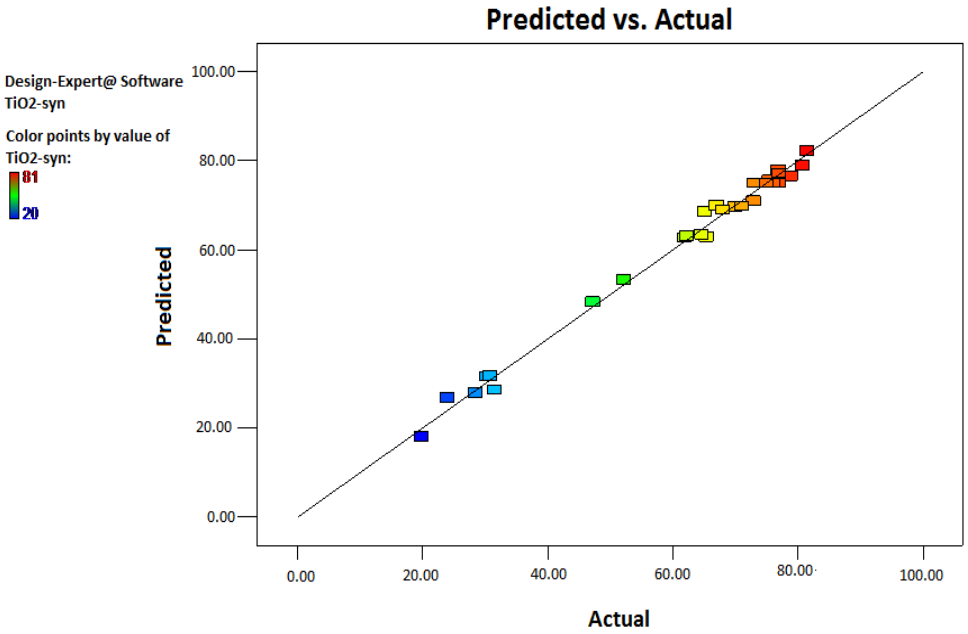

Fig. 6. Plot of actual data and predicted data

Table 4. Variance Analysis Results by using synthetic titanium dioxide

Source	Sum of Squares	df	Mean Square	F Value	P-value Probe>F
Model	10487.89	13	806.76	157.83	<0.0001 significant
A- Catalyst Loading	1657.79	1	1657.79	324.31	<0.0001
B- pH	812.50	1	812.50	158.95	<0.0001
C-C_{H2O2}	2439.71	1	2439.71	477.27	<0.0001
D- Air	1389.97	1	1389.97	271.92	<0.0001
AB	318.79	1	318.79	62.36	<0.0001
AC	718.88	1	718.88	140.63	<0.0001
AD	251.96	1	251.96	49.29	<0.0001
BC	838.46	1	838.46	164.03	<0.0001
CD	176.95	1	176.95	34.62	<0.0001
A^2	67.40	1	67.40	13.18	<0.0001
B^2	1411.51	1	1411.51	276.13	<0.0001
C^2	213.97	1	213.97	41.86	<0.0001
D^2	663.47	1	663.47	129.79	<0.0001
Residual	81.79	16	5.11	-	-
Lack of Fit	71.64	11	6.51	3.21	0.1043 not significant
Pure Error	10.15	5	2.03	-	-
Cor Total	10569.68	29	-	-	-

Adequate Precision=41.495, PRESS=411.40, R^2= 0.9923, Adjusted R^2= 0.9860,Pred R^2= 0.9611

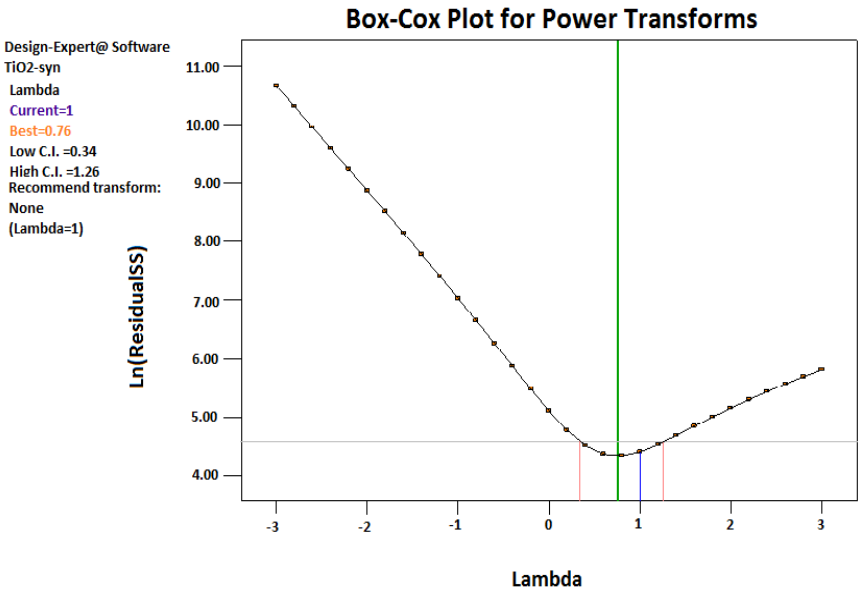

Fig. 7. Box-Cox Plot by using commercial titanium dioxide

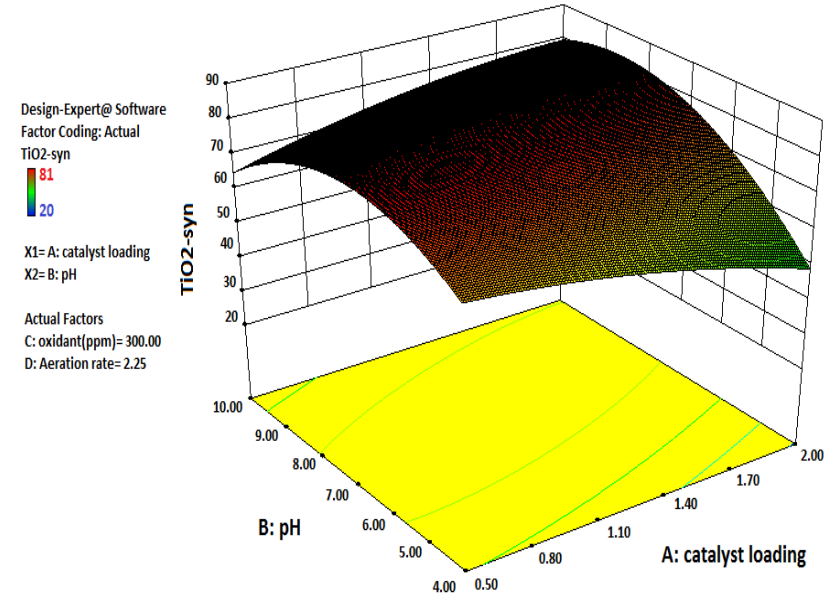

Fig. 8. Three-dimensional plots of the parameters change of the photocatalyst and pH values at different levels of auxiliary oxidant and for the middle value of aerated intensity, (A) Maximum value of oxidant auxiliary (B) Middle value of oxidant auxiliary (C) Minimum value of oxidant auxiliary

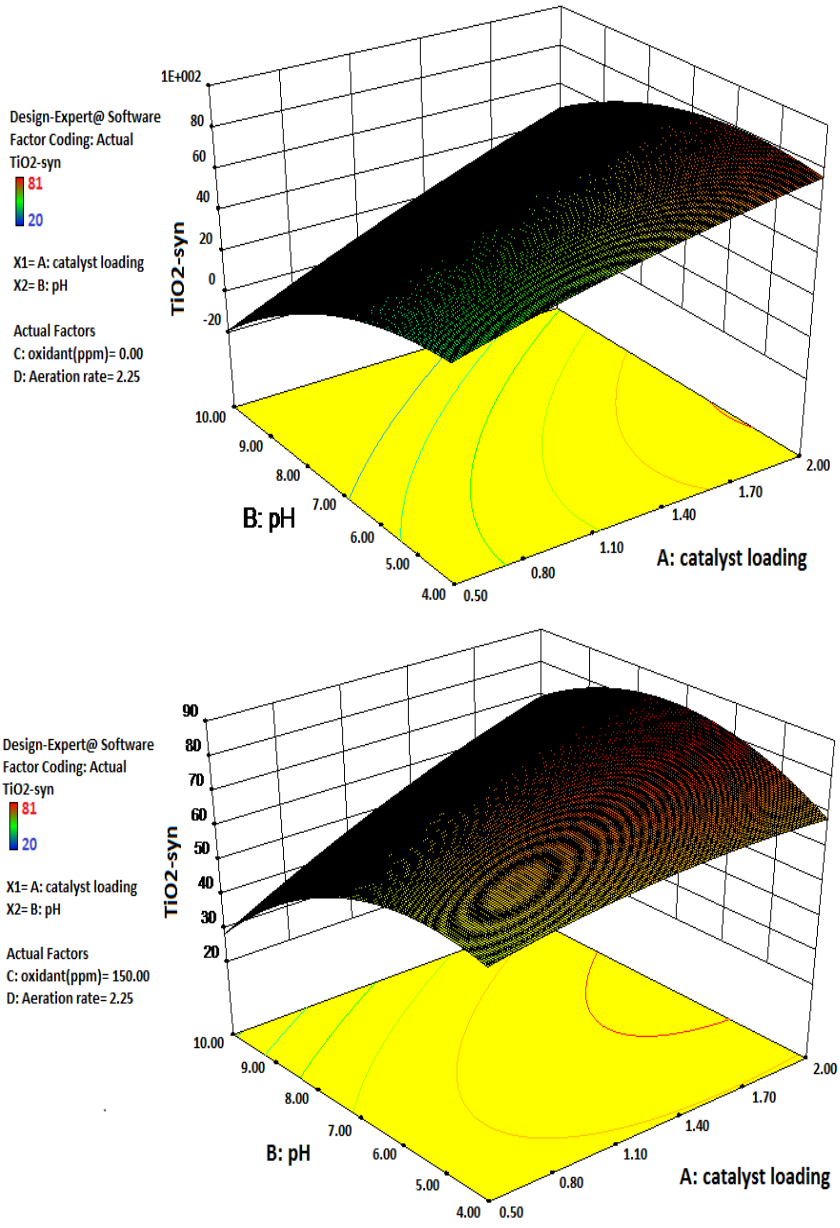

Fig. 8. (Continued)

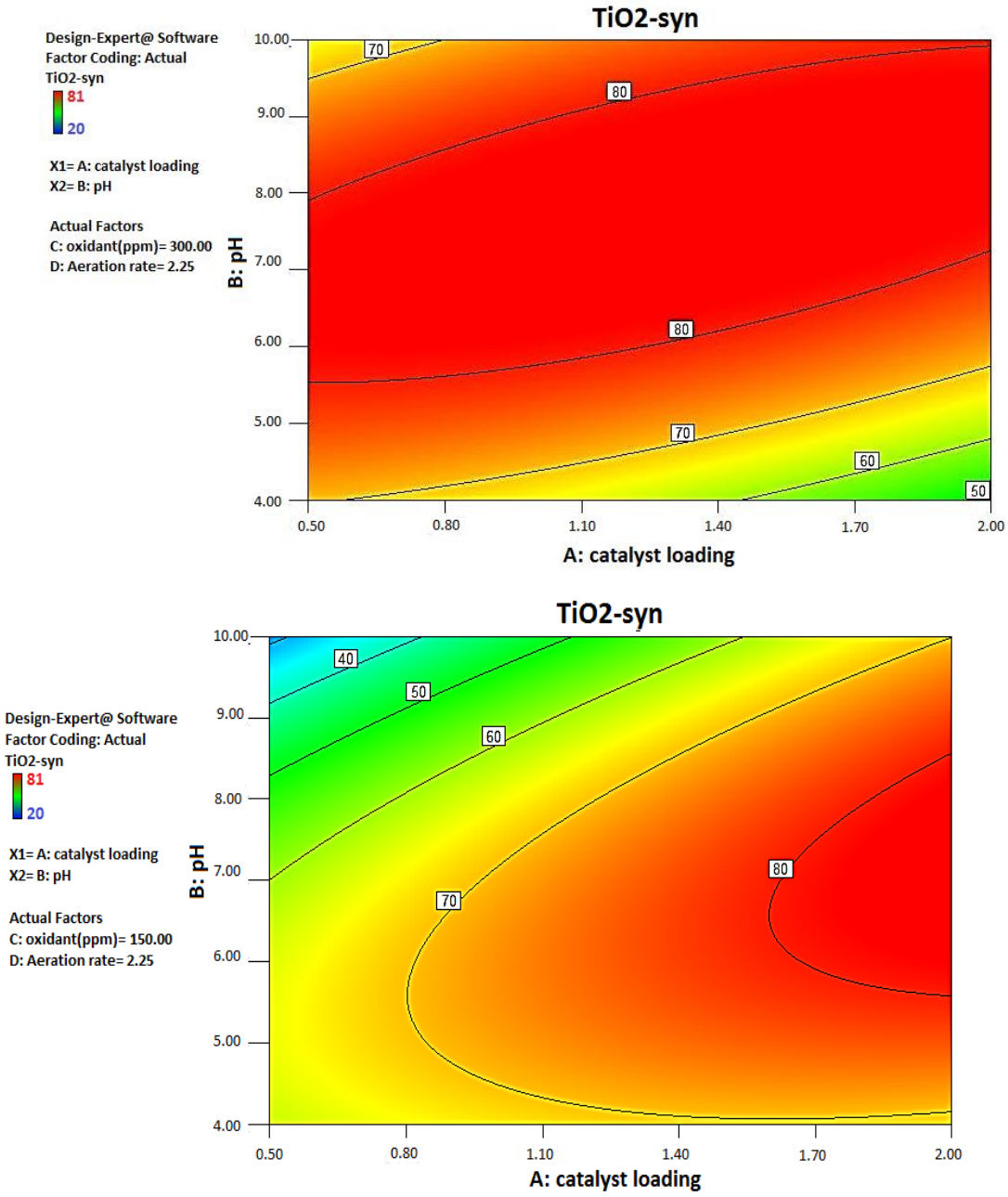

Fig. 9. The contour line plots of the parameters change of the photocatalyst and pH values at different levels of auxiliary oxidant and for the middle value of aerated intensity, (A) Maximum value of oxidant auxiliary (B) Middle value of oxidant auxiliary (C) Minimum value of oxidant auxiliary

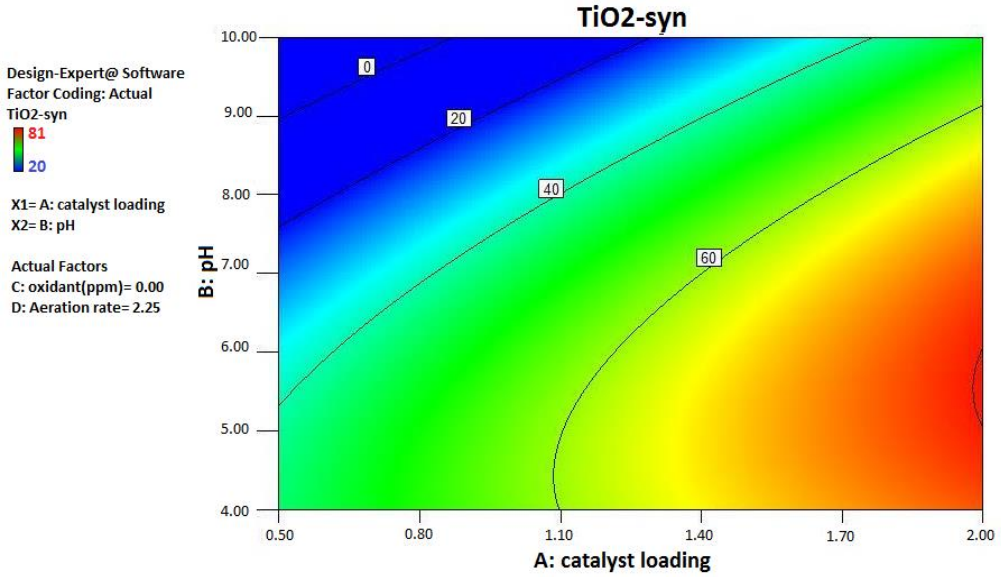

Fig. 9. (Continued)

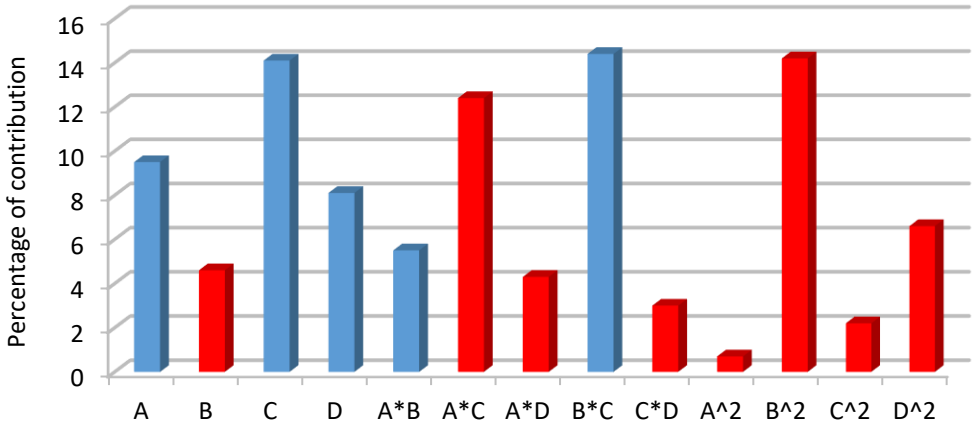

Fig. 10. Plot of percentage of the effect for each factor

3.1.4. Percentage plot of each factor effect

Figure 10 clearly shows that all factors, except pH, have a positive effect on the model. This means that if we do not consider the interactions, the efficiency will increase with the increasing of each factor (except pH).

3.1.5. Optimization

In this study, optimization is examined in two states: (1) without adjustment of the factor value that is the optimization without restrictions and (2) with adjustment of the selected parameters that is the optimization with restrictions. For optimization without the factor adjustment, all factors were placed in their limitation and the COD removal rate reached the maximum (Table 5). In Table 6, the result of the optimization of the model data was 81 percent. For optimization by adjusting the factors, the pH value factor was set on 7 and the using rate of the auxiliary oxidant was set to the minimum. As in the previous state, the COD removal rate was set to the maximum (Table 5). The obtained result of the optimization of the model data was 79% (Table 6).

Table 5. Optimizing the COD removal by software in two modes without restriction and with restrictions (Importance = 3)

Factor	High Intensity	Low Intensity	Objective	
			Without Restriction	With Restriction
A: Catalyst Loading	2	0.5	is in range	is in range
B: pH	10	4	is in range	is target=7
C: C_{H2O2}	300	0	is in range	minimize
D: Air	4	0.5	is in range	is in range
%COD	81	20	maximize	maximize

Table 6. Percentage of COD removal at the selected desirability point by model data for two states of without restrictions and with restrictions

Catalyst Loading	pH	C_{H2O2}	Air	%COD (model)	
1.31	7.04	247.31	3.18	81	With Restriction (Desirability=1)
2	7	0	3.09	79	Without Restriction (Desirability=0.95)

3.1.6. Comparison of the adoptions adsorption, photolysis and photocatalyst adoptions

The plot of Figure 11 provides a comparison between the adsorption, photolysis, and photocatalyst adoptions (without restriction conditions). As it was expected, the adsorption and photolysis processes in comparison to the photocatalyst adoptions had very little impact on COD removal efficiency and we can ignore it.

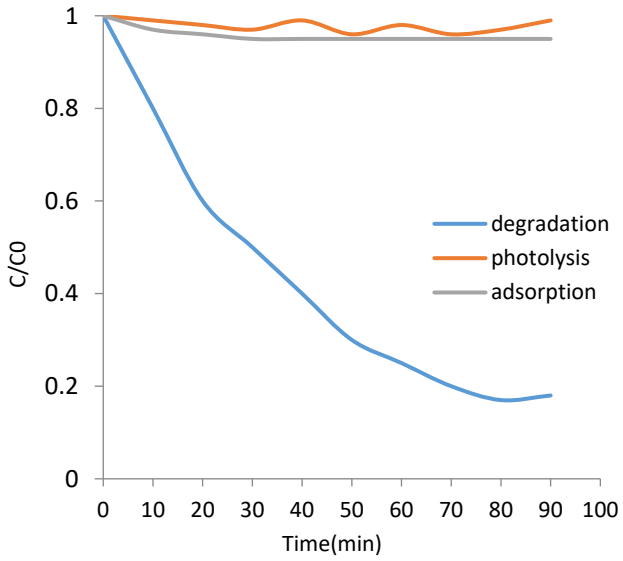

Fig. 11. Plot of comparison between the compatibles adsorption, photolysis and photocatalyst adoptions

3.1.7. Removal of the phenol in the wastewater sample

The plot of Figure 12 shows 80 percent of phenol removal in the wastewater sample during the test performance via the photocatalytic process under optimal conditions without restriction.

3.1.8. Sulfide removal in the wastewater sample

In this study, the removal of the existing sulfide percentage in the wastewater sample was reported to be 4.48% in 90 minutes and under the conditions with the middle value of determined limits for factors; this showed that the photocatalytic process had a negligible impact on the existing sulfide removal in the wastewater sample. But if it was assumed that the same small percentage of removal occurred via the adsorption process, it could be concluded that the photocatalytic process would not have more efficiency for the removal of inorganic compounds such as sulfide.

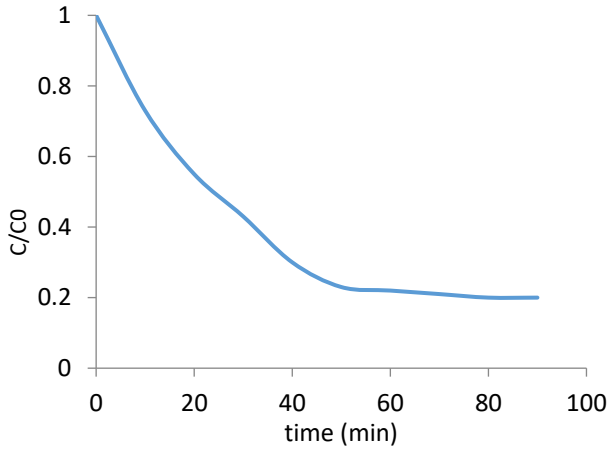

Fig. 12. Plot of phenol removal in wastewater sample

3.2. Artificial Neural Network Modeling

The neural network used in this study was the Single Layer Perceptron (SLP) which was trained as the feedback, so that only the input layer connected to the hidden layer and the hidden layer connected to the output layer. The training parameters and the data ranges of input and output variables are shown in Tables 7 and 8.

Table 7. Neural Network Training Parameters

Parameter	Value
Number of Inputs	4
Neuron Number of Hidden Layers	6
Number of outputs	1
Training method	Bayesian Regularization
Number of Epochs	1000
Hidden layer transfer function	Tansig
Output layer transfer function	Purelin
0.005	μ

To select the number of neurons, 2 to 20 neurons were considered each time in the hidden layer and the network was trained, and then the RMSE value was calculated. In Figure 13, the calculated RMSE value is shown for all the numbers of neurons. The number of neurons that obtain the least amount of RMSE was considered as the best structure; therefore, 6 neurons in the hidden layer were used to train the network. Notably, the training network was repeated 3 times for each structure to destroy the random results. The number of existing input and output data sets available for training the network are 30 in which

24 of them were used for training and 6 of them were used for validation. The obtained results from the neural network output are shown in the last column of Table 3. Figure 14 shows the laboratory output data in terms of the obtained results from the neural network. When the slope of the plot is close to 1, the accuracy of the model will be more; this importance has been achieved for the designed neural network. Also, given that the value of $R^{۲}$ =0.9976, it showed the high precision of the designed neural network.The two-dimensional contour plots shown in Figure 15 were used to study the effect of the considered parameters on the value of COD removal. As it can be seen in the plot in Figure 15a, the amount of COD removal is shown in terms of oxidant and aeration rate for a constant value of 7 and 1.25 for pH and loaded catalyst. Also, Figure 15b shows the amount of COD removal in terms of oxidant and pH for a constant value of 2.25 and 1.25 for aeration rate and loaded catalyst. In Figure 15c, the amount of COD removal is shown in terms of oxidant and loaded catalyst for the constant value of 2.25 and 7 for aeration rate and pH. In general, it can be concluded from this figure that increasing the oxidant leads to an increase in COD removal. According to Figure 15a, the COD removal rate increased by increasing the aeration rate for the amount of oxidant which was less than 150 ppm; otherwise, the COD removal decreased by increasing the aeration rate. It can also be said, according to Figure 15b, the pH parameter had a periodic effect on the COD removal percentage as follows: for pH values less than 6, the COD removal rate increased by increasing pH; otherwise, the COD removal rate decreased. It can be said with regard to Figure 15c, the COD removal rate increased by increasing the loaded catalyst.

Table 8. Model variables of neural network and their data range

Output layer	Removal value COD Experimental (%)	20-81
Input Layer	Aeration rate (L/min)	0.5-4
	Oxidant (ppm)	0-300
	pH	4-10
	amount Catalyst (g/L)	0.5-2

3.3. Comparison between qualitative parameters of both modeling

A comparison is made in Table 9 between the quality parameters of two modeling methods: DOE and ANN. It can be concluded that the neural network modeling was a more appropriate method than the DOE modeling to predict the amount of COD removal.

Table 9. Comparison between qualitative parameters of the DOE and ANN modeling methods

AAD	MAE	RMSE	Adjusted	R^2	Model
0.77	0.398	0.425	0.9860	0.9923	DOE
0.28	0.089	0.075	0.9910	0.9976	ANN

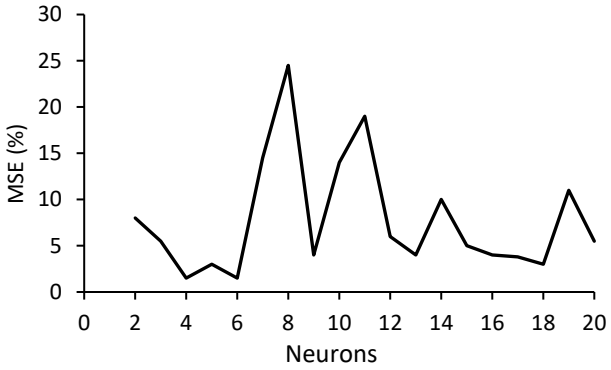

Fig. 13. RMSE value in terms of the number of neurons in the hidden layer

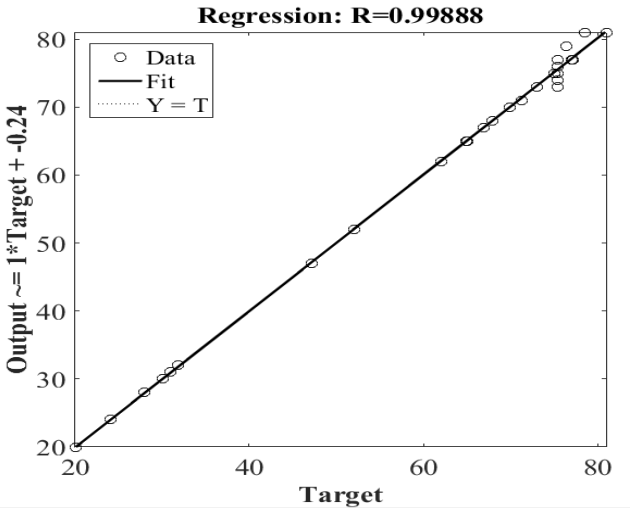

Fig. 14. Plot of laboratory output data based on the results of Artificial Neural Network

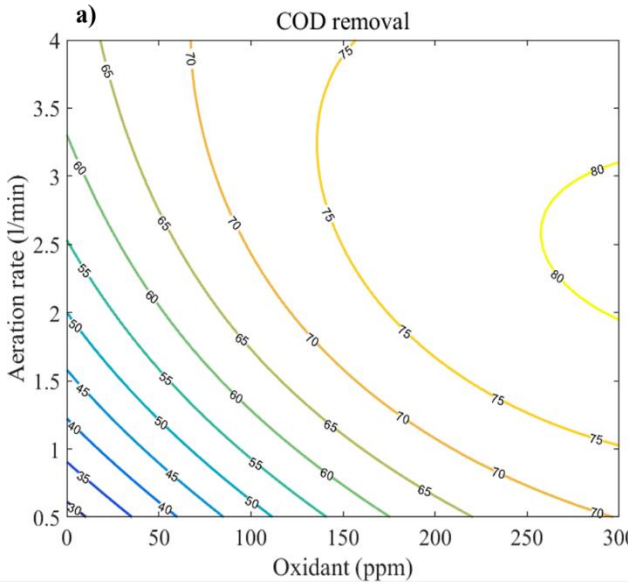

Fig. 15. Two-dimensional contour plot of COD removal based on the results of Artificial Neural Network

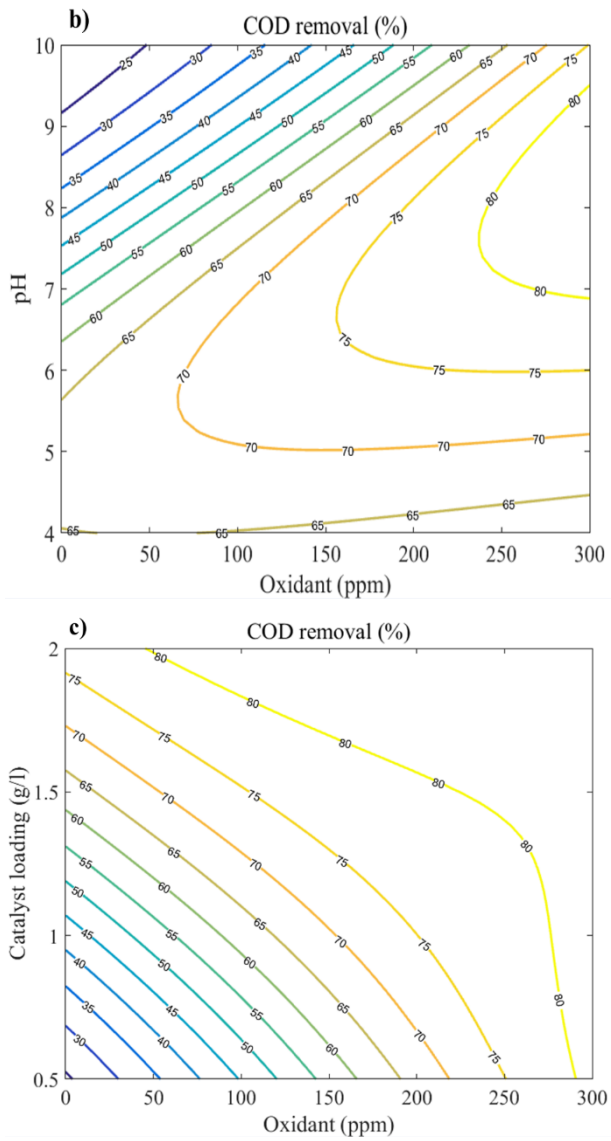

Fig. 15. (Continued)

4. Conclusions

In this study, the spent caustic in the wastewater of the Olefin units used in petrochemical industries was treated by using the photocatalyst method. For this purpose, a synthetic, suspended titanium dioxide photocatalyst was used in a double-cylindrical-shell photo reactor and the percentages of COD removed were measured alongside the existing phenol and sulfide in the wastewater sample. Then, the experimental results were compared via the Box-Behnken DOE and ANN models. The obtained results of both models showed a good adjustment with the experimental results. By comparing the qualities parameters of both models, it can be concluded that the ANN modeling was more appropriate to predict the amount of COD removal. In the modeling of this study, investigations on the effects of the oxidant parameters, aeration rate, pH and the amount of loaded catalyst on the amount of COD removal showed that all the factors had a positive effect on the model, except pH. This meant that if we did not consider the interactions, the efficiency would increase with the increasing of each individual factor (except pH). Also, there were no interactions between the aeration rate and the photocatalyst concentration. The study of the pH interaction and the photocatalyst concentration in the different amounts of the auxiliary oxidant showed that the existence of a high amount of oxidant retained the amount of removal at a high level. Also, when the oxidant was at its low level, we could see the efficiency reduction of the removal. The results showed that the adsorption and photolysis adoptions in comparison to the photocatalyst adoptions had very little impact on COD removal efficiency, and it can be ignored. Also, the photocatalytic method had an acceptable capability in removing the remaining phenol in the wastewater sample, whereas it was inefficient in reducing the dissolved sulfide in the wastewater.

References

[1] De Graaff, M., Bijmans, M. F., Abbas, B., Euverink, G. J., Muyzer, G., Janssen, A. J. (2011). Biological treatment of refinery spent caustics under halo-alkaline conditions. *Bioresource technology*, *102*(15), 7257-7264.

[2] Kumfer, B., Felch, C., Maugans, C. (2010, March). Wet air oxidation treatment of spent caustic in petroleum refineries. *In national petroleum refiners association conference, Phoenix, Arizona state* (Vol. 23).

[3] Carlos, T. M. S., Maugans, C. B. (2000, September). Wet air oxidation of refinery spent caustic: a refinery case study. In *NPRA conference, San Antonio, TX*.

[4] Sheu, S. H., Weng, H. S. (2001). Treatment of olefin plant spent caustic by combination of neutralization and Fenton reaction. *Water research*, *35*(8), 2017-2021.

[5] Rodriguez, N., Hansen, H. K., Nunez, P., Guzman, J. (2008). Spent caustic oxidation using electro-generated Fenton's reagent in a batch reactor. *Journal of environmental science and health Part A*, *43*(8), 952-960.

[6] Nunez, P., Hansen, H. K., Rodriguez, N., Guzman, J., Gutierrez, C. (2009). Electrochemical generation of Fenton's reagent to treat spent caustic wastewater. *Separation science and technology*, *44*(10), 2223-2233.

[7] Yu, Z. Z., Sun, D. Z., Li, C. H., Shi, P. F., Duan, X. D., Sun, G. R., Liu, J. X. (2003). UV-catalytic treatment of spent caustic from ethene plant with hydrogen peroxide and ozone oxidation. *Journal of environmental sciences (China)*, *16*(2), 272-275.

[8] Hawari, A., Ramadan, H., Abu-Reesh, I., Ouederni, M. (2015). A comparative study of the treatment of ethylene plant spent caustic by neutralization and classical and advanced oxidation. *Journal of environmental management*, *151*, 105-112.

[9] Abdulah, S. S., Hassan, M. A., Noor, Z. Z., Aris, A. (2011, September). Optimization of photo-Fenton oxidation of sulfidic spent caustic by using response surface methodology. In n*ational postgraduate conference (NPC), 2011* (pp. 1-7). IEEE.

[10] Chen, C. (2013). Wet air oxidation and catalytic wet air oxidation for refinery spent caustics degradation. *Journal of the chemical Ssociety of Pakistan*, *35*(2), 244-250.

[11] Alaiezadeh, M. (2015). Spent caustic wastewater treatment with electrical coagulation method. *The 1st international conference oil, gas, petrochemical and power plant.*

[12] Montgomery, D. (2012). Design and Analysis of Experiments. 6th ed., John Wiley and Sons.

[13] Haykin, S. (2008).Neural Networks: A Comprehensive Foundation.4th ed.,Prentice Hall PTR.

[14] Rehman, S., Ullah, R., Butt, A. M., Gohar, N. D. (2009). Strategies of making TiO_2 and ZnO visible light active. *Journal of hazardous materials*, *170*(2), 560-569.

[15] Rivera-Utrilla, J., Bautista-Toledo, I., Ferro-García, M. A., Moreno-Castilla, C. (2001). Activated carbon surface modifications by adsorption of bacteria and their effect on aqueous lead adsorption. *Journal of chemical technology and biotechnology*, *76*(12), 1209-1215.

[16] Standard methods for the examination of water and wastewater. *(2005).* in American Public Health Association (APHA):Washington, DC, USA, W.E. Federation and A.P.H. Association,Editors.

[17] Gaya, U. I., Abdullah, A. H. (2008). Heterogeneous photocatalytic degradation of organic contaminants over titanium dioxide: a review of fundamentals, progress and problems. *Journal of photochemistry and photobiology C: Photochemistry reviews*, *9*(1), 1-12.

[18] Nelofer, R., Ramanan, R. N., Rahman, R. N. Z. R. A., Basri, M., Ariff, A. B. (2012). Comparison of the estimation capabilities of response surface methodology and artificial neural network for the optimization of recombinant lipase production by E. coli BL21. *Journal of industrial microbiology and biotechnology*, *39*(2), 243-254.